Geometric and Electronic Structure of Amorphous Aluminophosphates. Ab Initio and Experimental Studies

Antonio M. Márquez,* Jaime Oviedo, and Javier Fernández Sanz

Departamento de Química Física, Universidad de Sevilla, Facultad de Química, E-41012 Sevilla, Spain

José J. Benítez and José Antonio Odriozola

Departamento de Química Inorgánica e Instituto de Ciencia de Materiales de Sevilla, Centro Mixto Universidad de Sevilla-CSIC, PO Box 874, E-41080 Sevilla, Spain

Received: July 2, 1997[⊗]

A combination of experimental (diffuse reflectance infrared Fourier transform spectroscopy, DRIFTS, and X-ray photoelectron spectroscopy, XPS) and ab initio studies of model clusters is used to understand the geometric and electronic structure of aluminophosphate (AlPO) systems used as catalytic materials. The presence of an intense IR band in the DRIFTS spectra, around 1300 cm^{-1}, together with literature data suggested to represent the system using cluster models based on metaphosphate-like structures. By varying the P/Al atomic ratio the basic features of $AlPO_4-Al_2O_3$ catalysts are modeled. The calculated geometrical parameters (bond distances and associated stretch force constants) are discussed in relation to the structure of the catalyst and, despite the inherent approximations in modeling solids with cluster models, fits quite well-the experimental X-ray data for aluminum metaphosphate. The computed ionization potentials (IP), O_{KVV} transitions, and IR spectra are in reasonable agreement with experimental data. The observed trends in XPS, continuous decrease of Al_{2p}, and P_{2p} and O_{1s} binding energies on decreasing the P/Al ratio are explained in terms of the alteration of the electronic density of the O atoms induced by the presence of Al as second neighbor of the P atom. A similar effect of this second neighbor lets us explain the modification of the O_{KVV} and DRIFTS data. As a result of these studies a model for the short-range structure of amorphous AlPO systems is proposed based on metaphosphate anions conected by layers rich in aluminum with γ-Al_2O_3-like structure.

1. Introduction

Amorphous aluminophosphates or AlPO systems, formally $AlPO_4-Al_2O_3$, have been shown to be highly efficient catalysts in a wide variety of processes including dehydrogenation,[1] cracking,[2] and isomerization[3] reactions, and as support for other catalytic systems such as oxides[4−6] or metals.[7] Their structure is usually described as built from $[AlO_4]$ and $[PO_4]$ tetrahedra as basic units and shows catalytic acidic properties that can be controlled by the modification of the Al/P ratio.[2] It has been shown recently that these systems are a precursor of a new solid phase with enhanced basic properties,[8−14] basic sites in the range $10.7 \leqslant pK_a \cong H_- \leqslant 11.2$.[14] This family of basic solids, also amorphous, are obtained without drastic modification of the textural properties of the precursors, indicating that after nitridation the basic local structure of aluminum and phosphorus is retained.

In the AlPO systems most of the characterization studies have shown the presence of tetrahedral phosphorus and aluminum cations but also of penta- and hexacoordinated aluminum cations.[1−7,15,16] In order to understand the parameters that may affect the nitridation process, the electronic and geometric structure of the precursor AlPO systems has to be known.

$AlPO_4-Al_2O_3$ systems are built up of $[PO_4]$ tetrahedra and $[AlO_4]$, $[AlO_5]$, and $[AlO_6]$ polyhedra. ^{27}Al MAS NMR data by Cheung et al.[37] show clearly the existence of penta- and hexacoordinated aluminum cations in the AlPO systems and also that the NMR spectra cannot be simulated by linear combinations of γ-Al_2O_3 and $AlPO_4$ solids. These authors, however, fail in providing a structural view of the AlPO solid. The existence of aluminum cations in coordination different from four, as should be expected for amorphous $AlPO_4$ systems, is also postulated by Rebenstorf et al.[4] through chemisorption and IR data. More recently, Babu et al.[1] reach the same conclusions with a series of amorphous aluminophosphate in which the precipitation and drying conditions were modified. So, the main conclusion of all these works is to determine that AlPO systems are not a mixture of γ-Al_2O_3 and $AlPO_4$ solids, but without providing alternatives. Early work by Cheung et al.[37] and Mitchell et al.[41] assume the existence of a phase alumina-like on decreasing the phosphorus content.

Molecular models of solids are adequate means of applying ab initio theoretical methods to understand solid-state problems. The reliability of the results from such ab initio studies is limited by the reduced size of the models and by inherent approximations of the theoretical methods used. In spite of these limitations, in recent years an increasing number of ab initio quantum chemical studies of solids and in particular of ionic oxides have been reported.[17,18] The reason is the interest in the theoretical description of the electronic properties of solids and the understanding of the relationship between structure and chemical properties which is relevant in materials science, catalysis, and solid-state chemistry.

In this paper we present a theoretical study, using ab initio techniques and model clusters to obtain structural information about the AlPO system. Geometric and electronic structure results are compared with experimental X-ray photoelectron spectroscopy (XPS) and diffuse reflectance infrared fourier transform spectroscopy (DRIFTS) data and available structural information on aluminophosphate systems[19,20] and are used to propose a structural model for amorphous AlPO systems.

* Corresponding author (email: marquez@quantix.us.es).

[⊗] Abstract published in *Advance ACS Abstracts,* November 1, 1997.

S1089-5647(97)02147-0 CCC: $14.00

2. Experimental Procedure

The sol−gel method developed by Kearby[21] is used to prepare high surface area amorphous oxide AlPO solids. At low temperature, 0 °C at most, 3 mol of propylene oxide per mole of aluminum are slowly added to a solution containing $AlCl_3 \cdot 6H_2O$ and H_3PO_4 in adequate amounts to obtain the desired P/Al ratios. At the end of the propylene oxide addition, the pH of the solution is increased to a value close to 3. After standing overnight at room temperature, the gel obtained is carefully washed with 2-propanol, dried, and calcined at 650 °C.

The XPS spectra were obtained from a Vacuum Generator 210 facility, 20 eV constant pass energy and Mg Kα radiation were used. Peak positions are adjusted to the spurious C_{1s} signal at 284.6 eV binding energy. Prior to the XPS analysis the samples were outgassed in a preparation chamber at 400 °C with a base pressure of 5×10^{-8} mbar.

DRIFTS spectra were collected from a controlled environment cell (Spectra-Tech 0030-101) equipped with ZnSe windows. The cell is mounted in a Nicolet 510P FT-IR spectrometer with a DTGS detector operated at 4 cm^{-1} resolution. A detailed description of this DRIFTS cell has already been given.[22]

3. Computational Details

Ab initio SCF calculations were undertaken using the standard 6-31G(d) basis set for all atoms. This basis set is known to yield geometries in good agreement with experimental values and vibrational frequencies of rather uniform quality.[23,24] The use of d-type polarization functions on the heavy atoms is a prerequisite for the adequate description of the bonding situation on these atoms. Particularly, it is mandatory for the correct description of the hypervalence of P atoms.

All geometries have been fully optimized at the RHF-SCF level by standard gradient techniques. The stationary points found were characterized as minima by fully analytical computation of the matrix of the second derivatives of the energy in a Cartesian representation. In order to obtain a set of physically meaningful force constants, this matrix was transformed into an internal coordinate representation. To avoid redundancies in the set of internal coordinates used for the six-membered rings, internal global coordinated were used for bending and torsional modes, as described by Pulay et al.[25] The full description of the internal coordinates and the internal global coordinates are available from the authors upon request.

All the calculations were performed using a parallel version of the HONDO-8.5 program[26−28] system running on a network of IBM RS6000 and HP/735 workstations.

4. Results and Discussion

Models. All the well-known polymorphic modifications of SiO_2 have their ordered counterparts in $AlPO_4$. In all of them each $[AlO_4]$ and $[PO_4]$ tetrahedron shares all four corners with other tetrahedra to give a three-dimensional network in which Al and P cations are ordered.[29] Aluminophosphates can be obtained with different stoichiometries, in particular $Al_4(P_4O_{12})_3$ was reported early,[19,20] and for this compound S_4 symmetry for the anion was proposed from Raman and IR data[30] in agreement with crystallographic X-ray data.[19]

Two main differences can be pointed out between the two structural types. First, the three-dimensional network in $AlPO_4$ polymorphs is made from Al−O−P links whereas in $Al_4(P_4O_{12})_3$ cyclic $P_4O_{12}^{3-}$ anions are present, resulting in P−O−P links. Second, as a consequence of these two structural types, phosphoryl groups (P═O) are present in the metaphosphate structure while they are absent in the tribasic orthophosphate.

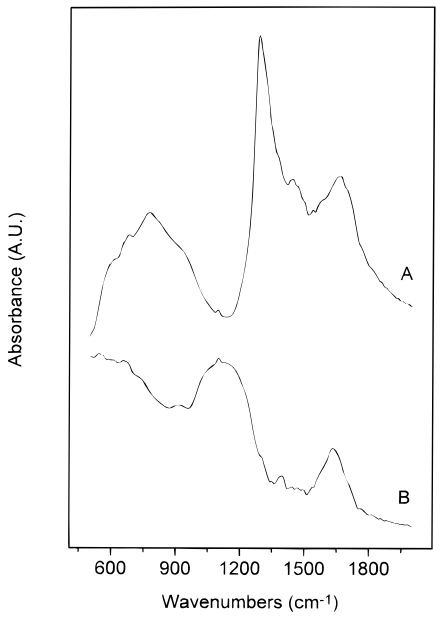

Figure 1. DRIFTS spectrum of an AlPO solid with P/Al = 1: (A) pure solid; (B) AlPO dispersion in KBr 12.5% w/w.

Usually, amorphous aluminophosphates (AlPO) are thought to present a local structure around aluminum and phosphorus similar to that present in $AlPO_4$, that is $[AlO_4]$ and $[PO_4]$ tetrahedra sharing all four corners and resulting in Al−O−P links within the solid framework. Unfortunately, no studies on the local structure and nature of the second neighbors that elucidate the possible controversy is known up to now. However, IR data on amorphous $AlPO_4-Al_2O_3$ systems showing bands around 1000−1100 cm^{-1} seem to justify this description.[31,32] More recently, by using DRIFTS data the presence of strong absorptions in these systems around 1300 cm^{-1} has been shown.[13,16] While bands at 1000−1100 cm^{-1} have to be ascribed to the existence of tribasic orthophosphate groups, bands in the 1300 cm^{-1} range are indicative of the existence of P═O bonds.[30] The discrepancy between data in refs 13 and 16 and data in refs 30 and 31 can be explained on the basis of the differences between transmission and reflectance spectroscopies.[33] Figure 1 shows the DRIFTS spectrum of an AlPO solid with P/Al = 1 once outgassed in the DRIFTS cell at 675 K; for comparative purposes the spectrum of the same sample is recorded, in reflectance mode, diluted in KBr (12% w/w). The existence of an intense *restrhalen* band around 1300 wavenumbers is evident in the DRIFTS spectrum of the pure solid, whereas the most intense bands appears at 1000−1100 wavenumbers once the solid is diluted in KBr. The spectrum of the diluted sample is similar to that previously reported for the $AlPO_4-Al_2O_3$ system by Bautista et al.,[31] which follows a similar dilution procedure for recording the spectrum. So, the existence of phosphoryl bands in these systems can be assumed, although, depending on the experimental procedure, they can be darkened in the spectrum which may lead to a misunderstanding of the local structure of the phosphorus atom.

On the other hand, AlPO solids have been synthesized in previous works as precursors of a novel basic catalyst family (AlPON).[8−14] During the nitridation process the textural characteristics of the precursor solid are not dramatically modified, suggesting the constancy of the local structure of the precursor after nitridation. Moreover, the structures of crystalline $AlNa_3P_3O_9N$ solids have been recently described.[34] This

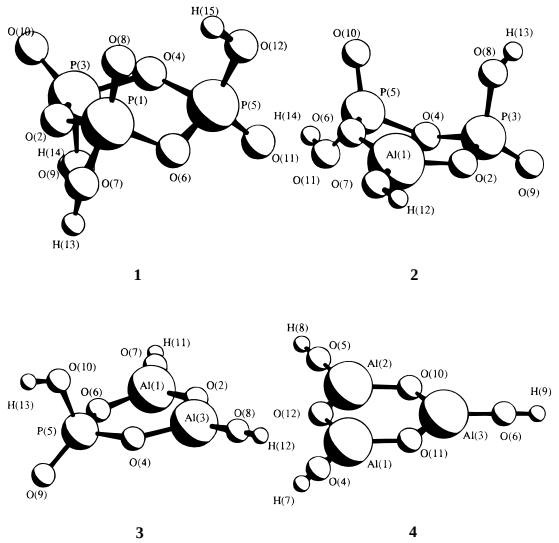

Figure 2. Molecular models of AlPO solid system.

solid presents a metaphosphate-like structure showing the existence of [PO_4] tetrahedra, [AlO_6] octahedra and P−X−P links (X = O, N). On the other hand, the existence of phosphazenes with a basic ring having P−N−P bonds is quite well-known.[35]

The choice of the model has to take into account the existence of phosphoryl groups and hence of P−O−P links within the solid as well as the varying P/Al ratios experimentally obtained. For this purpose, a six-membered ring starting with the trimetaphosphoric acid has been chosen, and the different P/Al ratios have been modeled by a progressive substitution of P atoms by Al atoms: Figure 2 (**1**, $P_3O_9H_3$; **2**, $AlP_2O_8H_3$; **3**, $Al_2PO_7H_3$; and **4**, $Al_3O_6H_3$). In these models the coordination polyhedra around phosphorus are always tetrahedral as stated in ^{31}P MAS NMR data[36] and also in accordance with NMR data for similar systems.[1,37] The coordination polyhedra around aluminum is, however, far away from reality, since the IR spectra of AlPO systems show the existence of tetrahedral, pentacoordinate, and octahedral aluminum cations within the solid framework.[1,4,16] However, any of these choices results in a negatively charged cluster which may influence the final results. Moreover, the important point for analyzing the experimental data is the effect of the second neighbor of the phosphorus atom. So, the first and second coordination spheres of phosphorus are properly modeled with the proposed clusters. This approach also opens comparison with future experiments on the geometric and electronic structure of AlPON solids already started in a previous work.[9]

Structure. A selected set of optimized bond distances are shown in Table 1. The P−OP distances (P−O with P in the second coordination sphere of the P atom) computed for model **1** range from 1.596 to 1.618 Å and both P−OP distances in model **2** are equal to 1.610 Å. These values suggest that the influence of the rest of the cluster in this bond is almost negligible. The same conclusion can be obtained comparing the P−OAl (P−O with Al in the second coordination sphere of the P atom) computed for molecular models **2** and **3**. Although there is a small difference in the values computed for this bond distance (1.561 Å for model **2**; 1.570 Å for model **3**), there seems to be very little influence of the rest of the skeleton on this bond. However, comparing P−OP and P−OAl bond distances, as can be seen, there is a large influence of the nature of the P atom second coordination sphere on the P−O distance, up to 0.058 Å. The substitution of the second neighbor P atom for the more electropositive Al atom results in a decrease of this bond length.

TABLE 1: Selected Bond Distances (Å)

	model **1**		model **2**		model **3**	model **4**
P−OP	1−2	1.601			1.610	
	1−6	1.600				
	3−2	1.604				
	5−6	1.619				
	5−4	1.613				
	3−4	1.596				
P−OAl				1.561	1.570	
Al−OP			1−6	1.707	1.718	
			1−2	1.713		
Al−OAl					1.686	1.698
P═O	1−8	1.442	3−9	1.440	1.449	
	3−10	1.434	5−10	1.444		
	5−11	1.431				
P−OH	5−12	1.555	3−8	1.584	1.594	
	3−9	1.571	5−11	1.576		
	1−7	1.551				
Al−OH				1.659	1.673	1.687

TABLE 2: Selected Stretch Force Constants (mdyn/Å)

	model **1**		model **2**		model **3**		model **4**
P−OP	1−2	5.89	4−5	5.55			
	1−6	5.92	3−4	5.57			
	2−3	5.82					
	5−6	5.49					
	5−4	5.54					
	3−4	6.00					
P−OAl				7.15		6.78	
Al−OP			1−6	4.59	1−6	4.31	
			1−2	4.49	3−4	4.36	
Al−OAl					1−2	5.12	4.86
					2−3	5.13	
P═O	1−8	12.66	3−9	12.83		12.27	
	3−10	13.18	5−10	12.56			
	5−11	13.33					
P−OH	5−12	7.53	3−8	6.69		6.62	
	3−9	7.05	5−11	6.88			
	1−7	7.63					
Al−OH				5.77		5.44	5.12

A similar trend can be extracted for the Al−O bond from the values computed for the Al−OP distances in compounds **2** (1.707 and 1.713 Å) and **3** (1.718 Å) and the Al−OAl distances in molecular models **3** (1.686 Å) and **4** (1.698 Å). Again, the substitution of the second neighbor P atom for Al results in a decrease in the bond length, about 0.03 Å.

In the monoclinic form of the aluminum metaphosphate there are nine different positions for the phosphorus atom, all of them corresponding to tetrahedral coordination. The four P−O distances are different, ranging from 1.468 to 1.593 Å.[20] The P−O distances in an averaged polyhedra are 1.479, 1.487, 1.573, and 1.585 Å. The aluminum cation are in octahedral coordination with Al−O distances ranging from 1.845 to 1.932 Å.[20] While the calculated values for the P−O distances are close to that found in the crystalline metaphosphate, the Al−O distances are shorter as corresponds to the reduced coordination number of aluminum in the calculated clusters. As an example, the Al−O distances in $AlPO_4$, where aluminum cations are in tetrahedral coordination, range from 1.606 to 1.740 Å depending on the structural polymorph. Although the P−O and Al−O distances in the cubic polymorph are slightly shorter than in the monoclinic one[19] the computed values for the P−O bond distances are still close to the experimental values.

Quite the same picture of the bonding situation is obtained when we look at the stretch force constants presented in Table 2. For compound **1**, the computed P−OP stretch force constants are between 6 and 5.49 mdyn/Å, similar to the values computed

TABLE 3: Koopman IP/eV

					O 1s	
	Al 2s	Al 2p	P 2s	P 2p	*a*	*b*
model **1**			209.9−209.5	152.7−152.3	559.5	561.7−562.5
model **2**	135.4	89.6−89.5	208.5	151.3	558.6	560.3−561.2
model **3**	134.2	88.4−88.3	207.6	150.4	557.8	559.4−560.4
model **4**	133.1	87.3−87.2				558.1−558.5

[a] Oxygens atoms from P═O groups. [b] Rest of oxygen atoms.

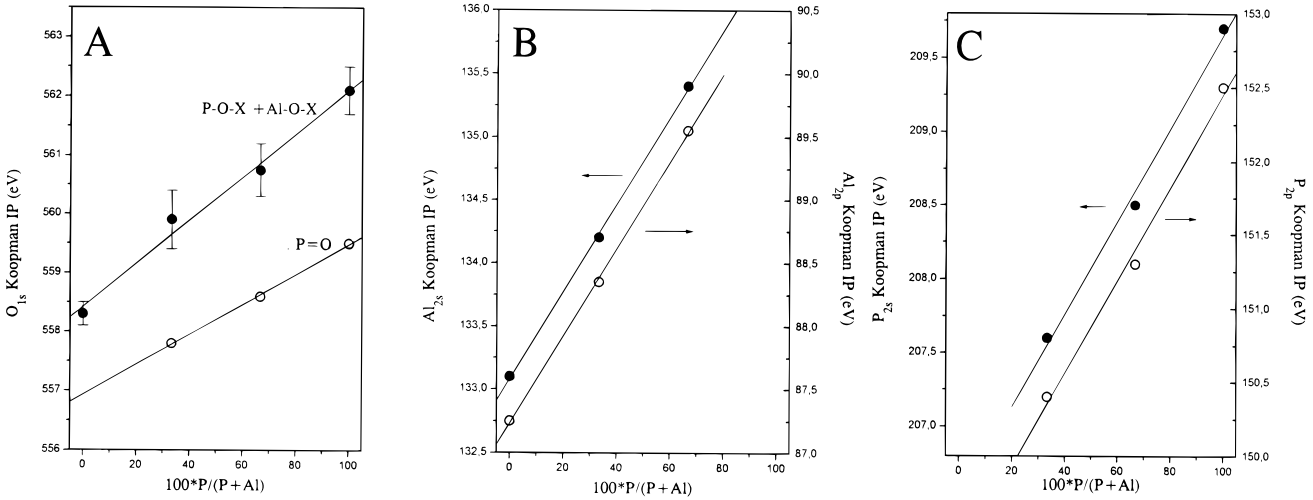

Figure 3. Variation of computed Koopman IP with atomic composition.

for compound **2**, 5.57−5.55 mdyn/Å. However, when the second neighbor P atom is substituted by an Al atom, the resulting force constant is much higher: 7.15 mdyn/Å in compound **2**, and 6.78 mdyn/Å in compound **3** for the P−OAl bond stretch. A parallel trend is found when the Al−O bonds are examined. While the computed bond stretch force constants for Al−OP bonds range from 4.49−4.59 mdyn/Å (model **2**) to 4.31−4.36 mdyn/Å (model **3**), there is a significant increase in the values computed for Al−OAl bonds, estimated to be 5.13−5.12 mdyn/Å in model **3**, and 4.86 mdyn/Å in model **4**.

Thus, the conclusion that can be drawn from both the decrease in bond lengths and the increase in the stretch force constants is that the substitution of Al atoms by P atoms in the AlPO catalyst results in a decrease of the strength of the network (longer bond distances and smaller force constants), mainly due to a second neighbor effect.

The next bond distance presented in Table 1 corresponds to the P═O bonds and the computed values range from 1.431 to 1.449 Å, showing practically no influence whatever on the rest of the molecular skeleton. The diagonal stretch force constants show a slight increase with increasing P/Al ratio, going from 12.27 mdyn/Å (**3**) to 13.33 mdyn/Å (**1**). The P−OH bond distances increase when the number of Al atoms increases. Their values go from 1.551 to 1.571 Å for model **1**, 1.576−1.584 Å for model **2**, and 1.594 Å for model **3**, thus showing an increase of 0.04 Å in the series. As a consequence, the associated stretch force constants decrease in the series, ranging from values of about 7.5 mdyn/Å for the stronger bonds in molecular model **1**, to 6.6 mdyn/Å for the single P−OH bond in model **3**. A similar trend is observed in the Al−OH bonds that increase from 1.659 Å in model **2** and 1.673 Å in model **3** to 1.687 Å in model **4**; and the associated force constants take the values 5.77, 5.44, and 5.12 mdyn/Å, decreasing in the series.

The behavior of the P═O and P−OH bond stretch force constants can be explained as a back-side effect of the observed increase in strength of the ring bonds discussed in the previous paragraph. While some electron density is reinforcing the ring bond, this density has to be taken from some other bonds (the P−OH and Al−OH bonds) which are consequently weakened (total bond order principle[38]).

Photoelectron Spectroscopy. The computed Koopman ionization potentials (IP) for different atomic orbitals are presented in Table 3. The absolute values of these IPs are not directly comparable to the experimental values since our calculations are molecular models that do not incorporate the effect of the relaxation of the hole, so the computed values are expected to be way off the experimental values by a few electrovolts. Instead, we will concentrate on examining trends by looking at the variation of these IP with composition. At first sight one sees that all IP decrease when going from molecular model **1** to **4**. Not only do these IP decrease but the lowering follows in all cases a linear dependency on the composition, expressed as a % of P (number of P atoms/total number of Al and P atoms) as shown in Figure 3. A similar trend is observed in the experimental data. Figure 4 shows the comparison between the experimental binding energies and calculated IPs, where the computed values have been averaged for better simulating the experimental XPS line that contains all the possible contributions without any feature that lets us deconvolute it. As previously stated the calculated IP are off the experimental values by around 15 eV, mainly due to the relaxation energy of the hole. Besides this, the full width at half-maximum (fwhm) of the core levels remains constant within ±0.1 eV for Al_{2s} (2.6 eV), Al_{2p} (2.2 eV), P_{2s} (3.2 eV), and P_{2p} (2.4 eV) whereas it goes from 2.4 to 3.3 for O_{1s} on decreasing the P/Al ratio. This modification of the fwhm values has to be associated to the different IP values obtained for P−O−H, P−O−P, and P−O−Al bonds present in the solid, as shown in Figure 3. The explanation of this behavior can be obtained by examining the composition of the corresponding molecular orbitals (MO) obtained from the RHF calculations. Although each MO is mainly atomic in character, more than 99% of the corresponding atomic orbital (AO) in each case, there is a small contribution from the rest of core AO. Thus the O_{1s} MO, for

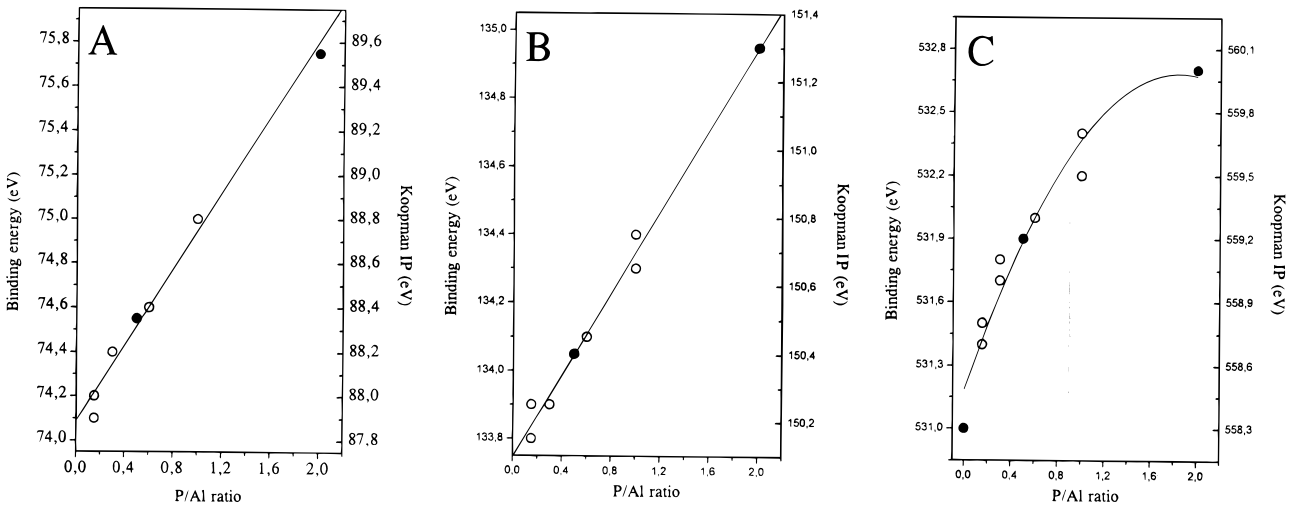

Figure 4. Variation of experimental binding energies and computed Koopman IP with the P/Al ratio: open symbols, experimental data; solid symbols, theoretical data.

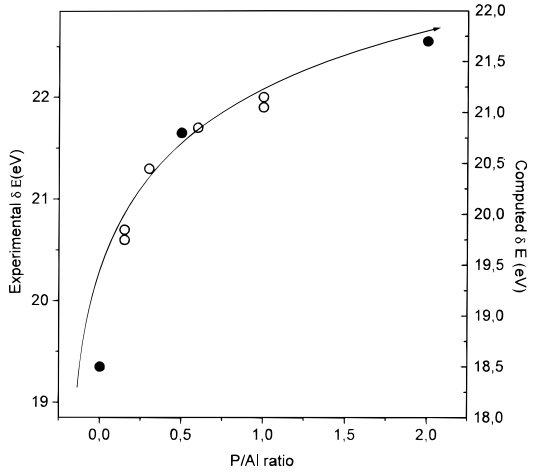

Figure 5. Variation of the energy difference between KL_1L_{23} and $KL_{23}L_{23}$ Auger lines for oxygen (δE) with the P/Al ratio: open symbols, experimental data; solid symbols, computational data.

example, has a small contribution from core AO from Al and P atoms and given that the P core levels are more energetic than those of Al, the net result is that the substitution of Al atoms by P atoms increases the Koopman IP of the MO representing the O_{1s} level. The same argument can be extended to the rest of MO examined. In other words, the bonding in these systems is not fully ionic, but some covalent component remains that mixes these AO and the increase in the P/Al ratio enhances the contribution of the P core levels to the MO that represent the different atomic levels increasing their binding energies.

The X-ray excited O_{KVV} spectra for the AlPO solids present, as their main feature, two peaks around 747 and 767 eV corresponding, respectively, to the $KL_{23}L_{23}$ and KL_1L_{23} oxygen transitions. A relationship between the energy separation of these lines (δE) and the ionic character of the oxygen bond has been previously reported by Wagner et al.[39] In their study over a wide series of oxides they claimed that an increment in the ionic contribution to the oxygen bond is characterized by a lowering in the energy separation between the oxygen $KL_{23}L_{23}$ and KL_1L_{23} lines. Figure 5 shows δE as a function of the P/Al ratio, an increment in δE on increasing the P/Al ratio is observed. The computation of KVV Auger spectra is not straightforward: the ejection of two valence electrons produces a multitude of configuration states which are mutually near degenerate, and this results in strong CI resonances. That being said, the simplest approach one can use is still based on the Koopman's theorem IPs. We have selected the MOs with the largest participation of the O_{2s} and O_{2p} AOs and the averaged value of the corresponding IP is taken as the center of the band, respectively, for each AOs. Then, we have computed the energy difference (δE) between the O_{2s} (L_1) and O_{2p} (L_{23}) levels in the four molecular models that can be related in that simple Koopman's approach to δE in the peaks observed in the experiment. The energies of the O_{2s} and O_{2p} levels obtained from the calculation as well as δE for each model are presented in Table 4 and δE is plotted against the composition in Figure 5. The same caution expressed with respect to the core IPs is in order here: the calculated IP will be off by a few electrovolts from the experimental values since relaxation effects have been neglected, in this case for the two holes. However, the experimental results are well reproduced by the calculation both in the trend and the values of δE. Examination of the values of the Koopman's IP for the O_{2s} and O_{2p} levels in Table 4 shows that both IP rise with increasing P loading but also that the largest increment appears in the O_{2s} level. The increment in the values of these IP can be explained by an argument similar to the one used in the previous section for the core level shifts. The substitution of an Al atom by a P atom in the coordination sphere of the O atom changes the composition of the MO representing these levels, increasing the participation of the P atomic levels, more energetic than those of the substituted Al atom. On the other hand, while the O_{2p} valence AO mixes with valence AOs from P and Al atoms of similar energies, the more energetic O_{2s} AO mixes with the more energetic AO from P and Al atoms where energy differences are bigger. Thus, the augmented covalency on the O bonds, with increasing participation of the more energetic P AOs leads to the computed shift of the O levels and to the increment of the energy difference δE.

TABLE 4: Koopman IP/eV

	O_{2s}	O_{2p}	δE
model **1**	39.7	17.1	22.3
model **2**	38.4	16.7	21.7
model **3**	37.0	16.2	20.8
model **4**	34.6	16.1	18.5

Infrared Spectroscopy. The computed vibrational spectra for the molecular models **1**−**4** are compiled in Table 5. The diagonal force constants in the computed force field have been scaled by 0.90 to obtain the displayed frequencies. This procedure is well established and attempts to account for

TABLE 5: Vibrational Spectrum (scalfc = 0.90)/cm^{-1}

	model **1**	model **2**	model **3**	model **4**	exp[a]
ν_{O-H}	3837	3965	4047	3949	3786
	3831	3856	3956	3948	3673
	3728	3852	3954		
$\nu_{P=O}$	1424	1388	1356		1347−50
	1406	1370			
	1379				
$\nu_{P-O} + \nu_{Al-O}$	1129	1115	1106	1008	1000−900
	1088	1100	1065	946	
	1056	1071	1060	933	
	1046	1046	976	870	
	1023	975	968		
	1000	957	934		
	976	940	873		
	954	916			
bendings	873	764	736	716	
	803	759	732	650	
	787	647	615	598	
	697	565	582	570	
	621	530	577		
	550	516	520		

[a] Experimental values from DRIFTS spectra.

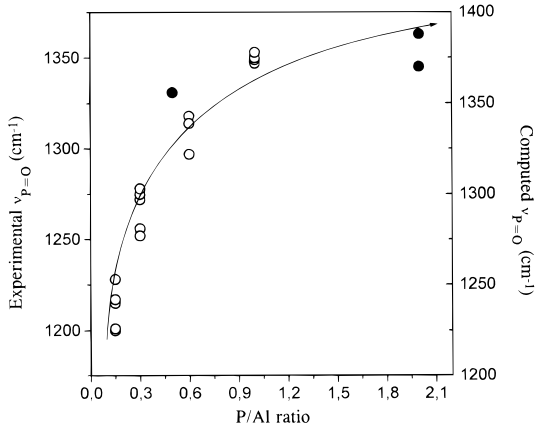

Figure 6. Variation of the P═O stretch frequency with P/Al ratio: open symbols, experimental data; solid symbols, theoretical data.

systematic errors in the force field computed at the RHF level, limited size of the basis set, and anharmonicity.

The computed vibrational spectra agrees with the experimental DRIFTS spectrum. The O−H stretch modes are computed at about 3730−3950 cm^{-1} while the experiment shows two main peaks at 3673 and 3786 cm^{-1} (for P/Al = 1), assigned to O−H groups bonded to P and tetrahedral Al atoms, respectively. The frequencies associated to P═O stretch modes are calculated between 1424 and 1356 cm^{-1}, showing a noticeable blue shift with increasing P/Al ratio in agreement with experimental observations, Figure 6. Note that in the experiment, the sample with the largest P/Al ratio (P/Al = 1.0) shows a peak in the DRIFTS spectrum at about 1347−1350 cm^{-1} that corresponds closely to the results of our calculations for models 2 (P/Al = 2; 1388, 1370 cm^{-1}) and 3 (P/Al = 0.5; 1356 cm^{-1}), so the agreement between the computed IR spectrum and the experiment can be said to be excellent. Similarly, for aluminum tetrametaphosphate, bands ascribed to phosphoryl groups are observed at 1311 and 1286 cm^{-1}.[40] Another consequence that can be extracted from the comparison between the computed spectrum and the experimental DRIFTS spectrum is that the observed peak should correspond to the stretch of P═O bonds that terminate the P coordination tetrahedra at the surface rather than to P−O bonds below the surface. The frequencies associated to the stretch of P−O and Al−O bonds appear in the computed spectrum in the range 1130−700 cm^{-1} and should correspond to the observed peaks in the DRIFTS spectrum around 1000−900 cm^{-1}, and observed for $Al_4(P_4O_{12})_3$ at 1083, 1066, and 1029 cm^{-1}.[40] The potential energy distribution (PED) analysis of the corresponding normal modes shows that it is almost impossible to separate the P−O and Al−O stretches; practically all vibrations are a mix of both and in the lower frequencies even a mixing with the bending modes appears. The computed frequencies shift toward higher values (100 cm^{-1}, approximately) when the P/Al ratio is increased in agreement with the trend discussed for the diagonal force constants ($f_{P-OAl} > f_{Al-OAl}$) and as a consequence, they also mix in the normal modes associated to the P═O stretch, displacing them to higher frequencies.

The agreement between experimental DRIFTS and XPS data and computational results assuming metaphospahe models using ab initio theoretical methods supports a new vision of amorphous aluminophosphate in which the solid is made of metaphosphate-like anions whose charges are compensated by aluminum cations. As the Al−O bond distances both in the monoclinic[20] and cubic[19] forms of the methaphosphate phase are close to that found in γ-Al_2O_3, the formation of alternating layers of methaphosphate and alumina leading to a more or less ordered framework can be envisaged.

5. Concluding Remarks

The combination of experimental (XPS and DRIFTS data) and ab initio studies on molecular models simulating metaphosphate solids provide an insight into the structure of AlPO catalysts.

The computed geometrical parameters (P−O and Al−O bond distances) fits the available experimental data quite well for the monoclinic and cubic polymorph forms of aluminum metaphosphate, supporting the choice of the molecular models for the short-range structure of the AlPO catalysts. The existence of an infrared band in the DRIFTS spectrum around 1300 wavenumbers that has to be ascribed to the stretch of P═O groups also points to the modification of the usual point of view about amorphous aluminophosphates.

The trends found in the computed Koopman's IP, O_{KVV} transitions, and IR spectra are in reasonable agreement with the experimental data. The observed continuous decrease of Al_{2p}, P_{2p}, and O_{1s} binding energies from XPS data on decreasing the P/Al ratio is explained in terms of the modification of the electronic density around the O atoms induced by the presence of P as second neighbhor of the Al atom. This second-neighbor effect also permits us to explain the observed variation of the O_{KVV} and DRIFTS data.

Acknowledgment. The authors thank the Centro de Estudios y Experimentación de Obras Públicas (CEDEX) for computational facilities. This work has been partially financed by the European Commission (Contract. No. ERCBT1-CT94-0064), by the Programa Iberoamericano de Ciencia y Tecnología para el Desarrollo (CYTED Project. No. V.4), and by the Spanish DGICyT (Proyect No. PB95-1247 and MAT94-0434-C03-02). A.M.M. thanks the Universidad de Sevilla for a grant.

References and Notes

(1) Babu, G. P.; Ganguli, P.; Metcalfe, K.; Rockliffe, J. W.; Smith, E. G. *J. Mater. Chem.* **1994**, *4*, 331.

(2) Campelo, J. M.; García, A.; Luna, D.; Marinas, J. M.; Romero, A. A.; Navío, J. A.; Macías, M. M. *J. Chem. Soc., Faraday Trans.* **1994**, *90*, 2265.

(3) Campelo, J. M.; García, A.; Luna, D.; Marinas, J. M. *J. Catal.* **1986**, *102*, 299.

(4) Rebenstorf, B.; Lindbland, T.; Andersson, S. L. *J. Catal.* **1991**, *128*, 293.

(5) Andersson, S. L. *Appl. Catal. A* **1989**, *112*, 209.
(6) Kuo, P. S.; Yang, B. L. *J. Catal.* **1989**, *117*, 301.
(7) Campelo, J. M.; García, A.; Luna, D.; Marinas, J. M. *J. Catal.* **1988**, *113*, 172.
(8) Marchand, R.; Conanec, R.; Laurent, Y.; Bastians, Ph.; Grange, P.; Gandía, L. M.; Montes, M.; Fernández, J.; Odriozola, J. A. Patent application FR 9401081.
(9) Grange, P.; Bastians, Ph.; Conanec, R.; Marchand, R.; Laurent, Y.; Gandía, L. M.; Montes, M.; Fernández, J.; Odriozola, J. A. *Stud. Surf. Sci. Catal.* **1994**, *91*, 389.
(10) Conanec, R.; Marchand, R.; Laurent, Y.; Bastians, Ph.; Grange, P. *Mater. Sci. Forum* **1994**, *152*, 305, Soft Chemistry Routes to New Materials, Nantes, France.
(11) Gandía, L. M.; Malm, R.; Marchand, R.; Conanec, R.; Laurent, Y.; Montes, M. *Appl. Catal. A* **1994**, *114*, L1.
(12) Grange, P.; Bastians, P.; Conanec, R.; Marchand, R.; Laurent, Y. *Appl. Catal. A* **1994**, *114*, L191.
(13) Benítez, J. J.; Odriozola, J. A.; Marchand, R.; Laurent, Y.; Grange, P. *J. Chem. Soc., Faraday Trans.* **1995**, *91*, 4477.
(14) Massinon, A.; Odriozola, J. A.; Bastians, Ph.; Conanec, R.; Marchand, R.; Laurent, Y.; Grange, P. *Appl. Catal. A* **1996**, *137*, 9.
(15) Moffat, J. B. *Catal. Rev.* **1978**, *18*, 199.
(16) Benítez, J. J.; Centeno, M. A.; Odriozola, J. A.; Conanec, R.; Marchand, R.; Laurent, Y. *Catal. Lett.* **1995**, *35*, 379.
(17) Sauer, J.; Ugliengo, P.; Garrone, E.; Saunders, V. R. *Chem. Rev.* **1994**, *94*, 2095.
(18) Sauer, J. *Chem. Rev.* **1989**, *89*, 199.
(19) Pauling, L.; Sherman, J. *Z. Krystallogr.* **1937**, *96*, 481.
(20) van der Meer, H. *Acta Crystallogr. B* **1976**, *32*, 2423.
(21) Kearby, K. *Proceedings of the 2nd International Congress on Catalysis*; (Technip: Paris, 1961; p 2567.
(22) Benítez, J. J.; Carrizosa, I.; Odriozola, J. A. *Appl. Spectrosc.* **1993**, *47*, 1760.
(23) Hariharan, P. C.; Pople, J. A. *Theor. Chim. Acta* **1973**, *28*, 213.
(24) Francl, M. M.; Pietro, W. J.; Hehre, W. J.; Binkley, J. S.; Gordon, M. S.; De Frees, D. J.; Pople, J. A. *J. Chem. Phys.* **1982**, *77*, 3654.
(25) Pulay, P.; Fogarasi, G.; Pang, F.; Boggs, J. E. *J. Am. Chem. Soc.* **1979**, *101*, 2550.
(26) Dupuis, M.; Johnston, F.; Márquez, A. HONDO 8.5 from CHEM-Station; IBM Corp., Neighborhood Road, Kingston, NY, 12401, 1994.
(27) Dupuis, M.; Chin, S.; Márquez, A. Modern Tools for Including Electron Correlation in Electronic Structure Studies: HONDO and CHEM-Station. In Relativistic and Electron Correlation Effects in Molecules and Solids; Malli, G. L., Ed.; NATO ASI Series; Plenum Press: New York, 1994.
(28) Márquez, A.; Oviedo, J.; Fernández Sanz, J.; Dupuis, M. *J. Comput. Chem.* **1997**, *18*, 159.
(29) Muller, O.; Roy, R. *The Major Ternary Structural Families*; Springer-Verlag: New York, 1974.
(30) Corbridge, D. E. C. In *Topics in Phosphorous Chemistry*; Grayson, M., and Griffith, E. J., Eds John Wiley and Sons: New York, 1989; Vol. 6, p 235.
(31) Bautista, F. M.; Campelo, J. M.; García, A.; Luna, D.; Marinas, J. M.; Romero, A. A. *Appl. Catal. A* **1993**, *96*, 175.
(32) Linblad, T.; Rebenstorf, B.; Yan, Z. G.; Larson, S. L. T. *Appl. Catal. A* **1994**, *112*, 187.
(33) Benítez, J. J.; Odriozola, J. A. Unpublished data.
(34) Conanec, R.; L'Haridon, P.; Feldmann, W.; Marchand, R.; Laurent, Y. *Eur. J. Solid State Inorg. Chem.* **1994**, *31*, 13.
(35) Cotton, F. A.; Wilkinson, G. *Advanced Inorganic Chemistry*, 5th ed.; J. Wiley: New York, 1988.
(36) Conanec, R. Ph.D. Thesis, University of Rennes I, 1994.
(37) Cheung, T. T. P.; Willcox, K. W.; McDaniel, M. P.; Johnson, M. M. *J. Catal.* **1986**, *102*, 10.
(38) van Santen, R. A.; Kramer, G. J. *Chem. Rev.* **1995**, *95*, 637.
(39) Wagner, C. D.; Zatko, D. A.; Raymond, R. H. *Anal. Chem.* **1980**, *52*, 1445.
(40) Corbridge, D. E. C.; Lowe, E. J. *J. Chem. Soc.* **1954**, 493.
(41) Mitchell, S. F.; Marcelin, G.; Goodwin, J. G. Jr. *J. Catal.* **1987**, *105*, 521.